FINAL REPORT

NASA Consortium, Cooperative Agreement NCA2-745

HYBRID LAMINAR FLOW CONTROL EXPERIMENTS IN THE NASA - AMES, 11-FOOT TUNNEL

To

Advanced Aero Concepts Branch
M-S 227-2
National Aeronautics and Space Administration
Ames Research Center
Moffett Field, California 94035-1000

JULY 1995

Submitted by

WILLIAM S. SARIC

Mechanical and Aerospace Engineering
College of Engineering and Applied Science
Arizona State University
Tempe, AZ 85287-6106
(602) 965-2822

Janice D. Bennett
Director, Office of Research Creative Activity
(602) 965-8239

ABSTRACT

It was proposed to design and conduct experiments in the NASA-Ames Research Center, 11-foot wind tunnel, that would assess the role of freestream turbulence and surface roughness on swept-wing transition to turbulence. The work was be a cooperative effort that had direct application to hybrid laminar flow control (HLFC) airfoils. The first part of the proposed work, initiated in FY92 and continued into FY93, concentrated on the design of such an experiment whose results may be compared with results obtained in other wind-tunnel facilities. At the same time, concurrent work in the ASU Unsteady Wind Tunnel would be conducted on the effects of surface roughness. The second part of the work, which was to be initiated in FY94, would have consisted of experiments conducted in both the 11-foot tunnel at NASA-Ames and the ASU Unsteady Wind Tunnel. However, this work was not continued. This report summarizes the experimental design considerations and some preliminary experiments that made up the first part of the work.

1. INTRODUCTION 1

1.1 Importance of Drag Reduction 1

1.2 Skin-Friction Reduction and Aircraft Design 2

1.3 Stability and Transition 3

1.4 Laminar Flow Control 4

1.5 Current Research Topics 5

2. CONCURRENT WORK: ASU ROUGHNESS EXPERIMENTS 6

2.1 Basic Experiment 6

2.2 Effect of Distributed Micron-Sized Roughness due to Surface Finish 8

2.3 Effect of Isolated Roughness Elements 9

2.4 Comparison with 2-D Boundary Layers 12

2.5 Summary 13

3. DESIGN CONSIDERATIONS 14

3.1 Design of the Model 14

3.2 Surface Roughness Experiments 15

4. REFERENCES 17

1. INTRODUCTION

The origins of turbulent flow and the transition from laminar to turbulent flow are the most important unsolved problems of fluid mechanics and aerodynamics. There is no dearth of applications where information regarding transition location and the details of the subsequent turbulent flow are extremely valuable. The one example that is applicable to this work, is skin-friction reduction on subsonic transports.

In this report, we first discuss the important application of *Laminar Flow Control* (or *LFC*) on the passenger transports commonly used today. Some recent research results in the area of transition to turbulence are reviewed and their importance to the application is shown. Because of the preliminary nature of this work, the author relies heavily on the following references which are to be considered the primary source material: Arnal and Michel (1990); Cousteix (1992); Gaster (1991); Hussaini and Voigt (1990); Morkovin (1983); Reshotko (1984); Thomas (1985).

1.1 Importance of Drag Reduction

Prior to the global fuel crisis of the early 1970's, fuel efficiency was only a minor feature of the design of civil air-transport systems (and automobiles). The trend in world fuel prices implies that now one can no longer ignore fuel efficiency in the design of aircraft. Indeed, the high fuel prices justify extraordinary means of fuel efficiency. For example, a 20% reduction in fuel consumption amounts to a saving of 10^8 liters of gasoline over a lifetime of a typical transport. At the price of gasoline these days, this could *pay* for a rather large aircraft. As another example, a new Boeing 747-400 has a take-off weight of 380,000 kg and a fuel load of 145,000 kg. A reduction of fuel by 25% saves 36,000 kg; this is on the order of the passenger payload.

Fuel consumption is, of course, related to total drag and it is possible to make the following ranking of drag of a generic aircraft.

1. Skin-friction drag due to the formation of the viscous boundary layer (typically turbulent) - *50% of total drag.*
2. Lift-induced drag due to the circulation established around finite-span wings - *35% of total drag.*
3. Pressure drag due to open separation in the afterbody and other regions - *8% of total drag.*

4. Interference effects between different aerodynamic components - *3% of total drag.*

5. Wave drag due to compressibility effects at near-sonic flight conditions - *2% of total drag.*

6. Roughness effects and leakage (miscellaneous) - *2% of total drag.*

Obviously the biggest target for drag reduction (and fuel savings) is the turbulent skin-friction drag. This is discussed in the next section. Work on control of separation through better configuration design and the reduction of induced drag through the use of winglets (the Boeing 747-400, Airbus A320, and Douglas MD-11 are examples) is continuing with some success.

1.2 Skin-Friction Reduction and Aircraft Design

There are two fundamental approaches to skin-friction reduction. The first is to maintain a laminar boundary layer and take advantage of the lower skin-friction coefficient and the second is to modify or restructure the turbulence within the boundary layer by means of changing surface conditions. When comparing laminar and turbulent boundary layers it is important to note that the turbulent skin-friction coefficient is at least 5 times greater than the laminar case over the entire Reynolds number range. Sustaining a laminar boundary layer in order to take advantage of an 80% reduction in skin friction is called laminar flow control or *LFC*. Just being able to sustain laminar flow to 75% chord on the wings results in a 25% reduction in fuel. It is unlikely, for a number of reasons, that laminar flow can be maintained on the fuselage or the empennage. In these areas, turbulent skin-friction reduction by means of riblets can be achieved on the order of 6%. The topic of modifying turbulence is another area of active research.

It is important to emphasize that skin-friction reduction is only a part of an energy efficient aircraft. If one considers the overall design requirements, the features of an energy-efficient aircraft will have the following characteristics:

1. Super-critical airfoils
2. LFC
3. Turbulent drag reduction
4. Winglets
5. High-aspect-ratio wings with trusses
6. High by-pass engines

7. Unducted fans

Thus, laminar flow control is only one part of the complete design problem. It should be obvious that one cannot separate aerodynamic design from the structural design and the propulsion requirements.

1.3 Stability and Transition

The role of LFC is to keep the boundary layer laminar and avoid the occurrence of transition. The boundary-layer transition problem consists of three important phases -- receptivity, linear disturbance amplification, and nonlinear interaction and breakdown (Arnal, 1992; Saric, 1986, 1992). The Navier-Stokes equations are the appropriate model for all of these phases. However, techniques to solve these equations for the entire range of the transition problem are only now being developed. Most experimental and theoretical examinations are presently focused on the second of the phases -- linear disturbance growth in a laminar boundary layer. It is this region where laminar flow control is effective.

The process of laminar-turbulent transition is generally the result of the uncontrolled growth small disturbances. A number of instability mechanisms may be in operation within the boundary layer on the surface of a wing. They are (1) streamwise instabilities, (2) crossflow instabilities, (3) curvature induced instabilities, and (4) attachment-line instabilities.

The streamwise instability is a viscous instability wave called a *Tollmien-Schlichting* (T-S) wave. These waves are initially two-dimensional and are selectively amplified or damped depending on Reynolds number and frequency. This instability is most important in the mid-chord region where the C_p distribution may be flat or decelerating. This mechanism is reviewed by Arnal (1992) and Saric (1985a, 1992).

A second type of instability results when a three-dimensional flow exhibits an inflection velocity profile (in this case due to crossflow on swept wings). The initially favorable pressure gradient over the swept airfoil deflects the inviscid streamlines inboard. Because of viscosity, the deflection is greater inside the boundary layer giving rise to a component of velocity perpendicular to the inviscid streamlines that is called the *crossflow* velocity. This profile undergoes a dynamical instability which becomes more important as sweep angle increases. It dominates in the leading-edge region where the crossflow is maximal due to favorable pressure gradients. Thus it is amplified by favorable pressure gradients. This instability is characterized by streamwise vortices all having the same sense

of rotation that are called *crossflow vortices*. The details of this mechanism are reviewed by Reed and Saric (1989).

Another type of dynamical instability that can occur, depends on the nature of the wall curvature. The presence of concave curvature and the accompanying centrifugal forces give rise to the *Görtler* instability (Saric, 1994). In this case the instability is in the form of counter-rotating vortices. Finally, there is the case of leading-edge contamination and attachment-line stability which involves the propagation along the attachment line of disturbances that originate from local disturbances or from the turbulent boundary layer on the fuselage. This is called the *Pfenninger* instability (Reed and Saric, 1989).

1.4 Laminar Flow Control

The principle behind LFC is to keep the growth of these disturbances within acceptable limits so that 3-D and nonlinear effects do not cause breakdown to turbulence. With this philosophy, one only deals with linear disturbances and thus, the difficulties with transition prediction do not arise.

Linear stability is governed by the linearized, unsteady Navier-Stokes equations in the form of what is called the Orr-Sommerfeld equation. It is well known that the velocity-profile curvature term in the Orr-Sommerfeld equation, $-\mathrm{d}^2U/\mathrm{d}y^2$, is *the* important driver of the stability behavior. The boundary layer can be made to be *more stable* by making the profile curvature *more negative* near the wall. The boundary-layer momentum equation can be evaluated near the wall, as shown in Eq. (1) and used to illustrate the stabilizing effects of different LFC techniques (Saric, 1985b, 1992).

$$\rho V_o \frac{\partial U}{\partial y} + \frac{\partial P}{\partial x} - \frac{\mathrm{d}\mu}{\mathrm{d}T}\frac{\partial T}{\partial y} = \mu \frac{\partial^2 U}{\partial y^2} \quad \text{as} \quad y \to 0 \tag{1}$$

Here, ρ is the density, V_o is velocity normal to the wall at the wall (+ for blowing, - for suction), U is the streamwise velocity component, P is the pressure field, μ is the dynamic viscosity, T is the temperature, x is the streamwise coordinate, and y is the wall-normal coordinate.

Equation (1) shows that wall suction ($V_o < 0$), favorable pressure gradient ($\partial P/\partial x < 0$), cooling in air ($\mathrm{d}\mu/\mathrm{d}T > 0$, $\partial T/\partial y > 0$), and heating in water ($\mathrm{d}\mu/\mathrm{d}T < 0$, $\partial T/\partial y < 0$), all tend to stabilize the boundary layer by making the profile curvature more negative.

It should be pointed out that these are very sensitive mechanisms and that even *weak* suction or *weak* pressure gradients produce strong effects. For example, a Falkner-Skan

pressure gradient of $\beta = +0.1$ (which can be measured by comparing a 6.6% change in the shape factor δ^* / θ with a Blasius boundary layer), increases the minimum critical x-Reynolds number for stability by a factor of 9. At the same time, average suction velocity ratios of $V_o / U_\infty \approx 10^{-3}$ or 10^{-4} are not unusual for LFC applications and can, for example, reduce relative amplitude growth from e^{26} to e^5 at low frequencies (Saric and Nayfeh, 1977). That the system works is evidenced by the fact that the X-21 aircraft achieved laminar flow at chord Reynolds numbers of 27×10^6 with a 20% decrease in overall drag.

Present designs for super-critical energy-efficient airfoils have LFC systems with a porous region near the leading edge of a swept wing in order to control leading-edge contamination and crossflow instabilities. Appropriate shaping of the pressure distribution stabilizes mid-chord instabilities. This arrangement has been called *hybrid* LFC because it combines *active* LFC (suction) with *passive* LFC (pressure gradient).

1.5 Current Research Topics

The details of the actual research programs that are being conducted at Arizona State University are beyond the scope of the preliminary report. It is possible however, to give a brief overview of the topics being addressed at ASU.

1.5.1. Secondary instabilities and nonlinear stages of crossflow vortex breakdown: Experimental, theoretical, and computational programs are progressing in order to study the nature of the initial stages of the transition region. A new type of instability has been discovered (Kohama et al. 1991) and indications are that the transition prediction schemes for crossflow-dominated transition must be changed (Reed and Fuciarelli, 1991).

1.5.2. Effect of micron-sized roughness on crossflow transition: We have shown that surface roughness near the attachment line of a swept wing that is the order of less than a micron (roughness Reynolds numbers less than one) has a profound effect on transition location (Radeztsky et al. 1993). This forces a reconsideration of surface-finish requirements as well as a reassessment of the insect deposition problem.

1.5.3. Interaction of sound with 2-D and 3-D surface roughness and with different leading edges: The interaction of sound and surface roughness and leading creates unstable T-S waves in the boundary layer (Saric et al., 1991; Radeztsky et al., 1991; Spencer et al., 1991). The details of this problem are being studied in order to understand how unstable waves appear in the flow. These studies include model studies in a towing tank to examine the structure of the flow field over small roughness elements and sensitive wind-tunnel

experiments to examine the stability characteristics (Saric et al., 1990). Navier-Stokes simulations are also progressing (Lin et al., 1991).

1.5.4. Stability of supersonic and hypersonic boundary layers: These are theoretical and computational studies of laminar flow control for high speed civil transport and for hypersonic vehicles. The three dimensionality of the mean flow is important as well as the chemical reactions that occur inside the high-temperature boundary layer. The stability calculations are now being conducted at ASU (Reed et al., 1992).

2. CONCURRENT WORK: ASU ROUGHNESS EXPERIMENTS

The goal of the present investigation is to determine the fundamental nature of the crossflow instability that is characteristic of the breakdown of swept-wing flows. This work feeds directly into the NASA-Ames supported work. Reviews of the current literature and problems are given by Reed and Saric (1989), Arnal (1992), and Saric (1992).

2.1 Basic Experiment

The present work is the result of an ongoing experiment on three-dimensional boundary layers. We have already documented the basic stability work which includes the wavelengths, local growth rates, frequencies, and evolution patterns of the crossflow vortices in the linear range (Saric et al. 1989; Dagenhart et al. 1989, 1990; Dagenhart 1992). In this work, the frequencies of the crossflow instability are observed to establish the existence of the theoretically-predicted moving crossflow vortices in addition to stationary crossflow vortices. The nonlinear processes that control transition have been documented by Kohama et al. (1991).

The NLF(2)-0415 airfoil (Somers and Horstmann 1985) that is used in this experiment has a pressure minimum on the upper surface at approximately $x/c = 0.71$. Wall liners within the tunnel produce an infinite-swept-wing flow with no spanwise gradients. With a 45° sweep and a small negative angle of attack, this favorable pressure gradient prevents T-S wave formation at moderate chord Reynolds numbers, but produces considerable crossflow. This permits the isolated examination of the crossflow stability problem. The instability at $\alpha = -4°$ was analyzed using the MARIA and SALLY stability codes. At a chord Reynolds number of $Re_c = 3.8 \times 10^6$, the maximum predicted N-factor is $N = 16.0$ for $f = 200$ Hz. Dagenhart (1981) indicates that transition may be expected for N-factors in the range from 9 to 11. Thus, for sufficiently high Reynolds numbers (less than 3.8×10^6), the transition due to crossflow vortex amplification is expected to occur

well ahead of the pressure minimum at $x/c = 0.71$. The fundamental linear stability results for this configuration are given by Dagenhart et al. (1989, 1990) and Dagenhart (1992). The secondary instability that leads to transition is described by Kohama et al. (1991).

One of the key missing ingredients in all 3-D boundary-layer experiments is the understanding of *receptivity*. Here, receptivity refers to the mechanisms that cause environmental disturbances to enter the boundary layer and cause unstable waves (e.g. Saric et al. 1991). Receptivity has many different paths through which to introduce a disturbance into the boundary layer. They include the interaction of freestream turbulence and acoustical disturbances (sound) with model vibrations, leading-edge curvature, discontinuities in surface curvature, or surface roughness. Any one or a combination of these may lead to unstable waves in the boundary layer. If the initial amplitudes of the disturbances are small they will tend to excite the linear normal modes of the boundary layer.

Whereas linear stability theory predicts that the traveling crossflow waves are more amplified than the stationary crossflow waves, many experiments observe stationary waves. The question of whether one observes stationary or traveling crossflow waves is cast inside the receptivity problem. Bippes and Müller (1990) and Bippes (1991) describe a series of comparative experiments in a low-turbulence tunnel and a high-turbulence tunnel. Their results show that traveling crossflow waves are observed in the high-turbulence tunnel rich in unsteady freestream disturbances and the dominant structure in a low-turbulence tunnel is a stationary crossflow vortex. Since the flight environment is more benign than the wind tunnel, one expects the low-turbulence results to be more important.

Our previous work showed that detailed measurements within the boundary layer can reveal both the traveling and stationary waves according to linear theory. However, our recent work (Kohama et al. 1991) showed that even though the traveling wave is more highly amplified, the meanflow distortion due to the stationary vortex induces a high-frequency secondary instability that leads to transition. Thus, crossflow transition is determined by the characteristics of the stationary wave.

The receptivity problem for stationary vortices is cast within sources of streamwise vorticity. We have shown (Saric et al. 1990) that even in the Stokes-flow limit, the flow around a small roughness within a shear layer separates and is a source of vorticity. Thus the present work concentrates on the role of surface roughness in influencing swept-wing transition.

2.2 Effect of Distributed Micron-Sized Roughness due to Surface Finish

The results are obtained from naphthalene flow visualization. This technique relies on the sublimation patterns of the naphthalene to identify the stationary crossflow structure and the location of transition. This technique was calibrated in previous experiments by the use of surface-mounted hot films (Dagenhart et al. 1989; Mangalam et al. 1990). Surface roughness measurements were done by taking castings of the surface with a *dental pattern resin* which created a rigid sample suitable for profilometer measurements.

The transition location, x_{tr}/c, was observed to increase with subsequent levels of polishing of the model. The original experiment had a painted model and the peak-to-peak roughness was around 8 to 10 μm. Transition experiments were conducted at a number of different chord Reynolds numbers, Re_c. The model surface was then polished to 0.5 μm rms finish and the experiments were repeated. The model was then subjected to a systematic hand-polished effort and the surface was brought down to a 0.25 μm rms finish. The results are shown in Figure 1. The painted surface results are from Dagenhart et al. (1989). The polished surface results show the effect of surface finish.

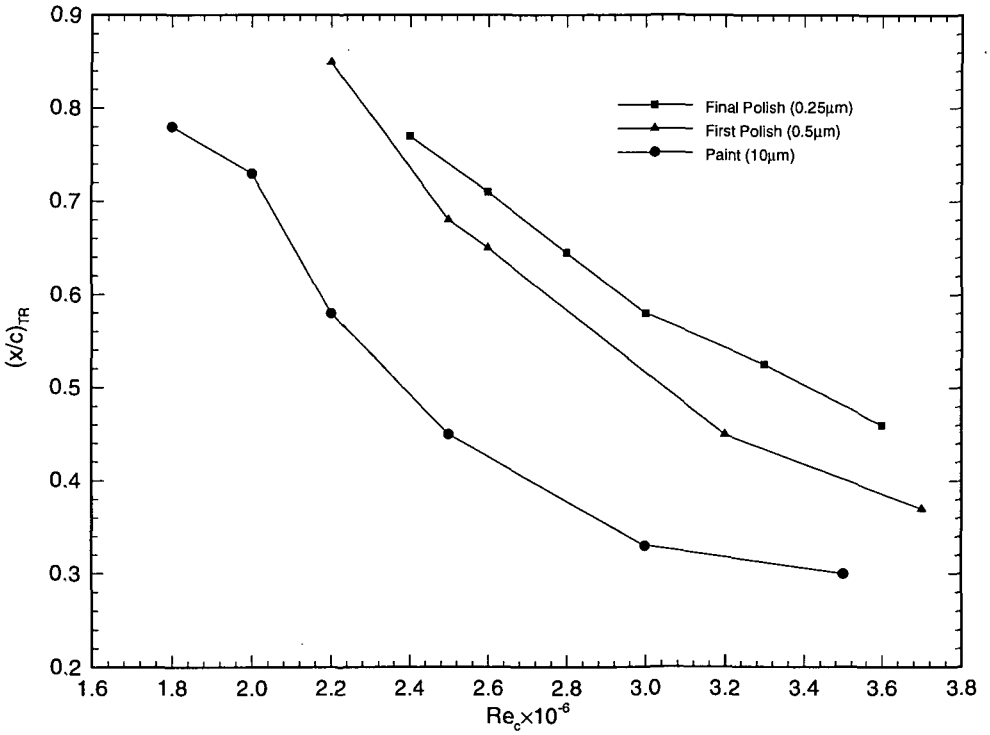

Figure 1. Naphthalene flow-visualization measurements of average transition location with three different surface finishes and α = -4°.

On the next page, Table 1 is an example of the data from one typical chord Reynolds number.

Table 1. Transition location as a function of roughness height. k is the nominal roughness height in microns, x_{tr}/c is transition location, $N(\omega = 0)$ is the amplification factor for most amplified stationary crossflow wave, and N is amplification factor for the most amplified traveling wave. Re_k is the roughness Reynolds number based on k and the velocity at that height. $Re_c = 2.7 \times 10^6$

k [μm]	x_{tr}/c	$N(\omega = 0)$	N	Re_k
9	0.40	5.5	7.1	0.30
0.5	0.61	8.4	11.0	$< 10^{-3}$
0.25	0.68	9.2	11.8	$< 10^{-3}$

It may be just a coincidence, but the stability amplitude ratios are in the proportion 1:18:40 while the initial amplitudes of the surface roughness are in the proportion of 1:1/18:1/36 near the leading edge. This initially suggests that a *quantitative* measure of stability/transition N-factor may be determined from surface roughness. These dramatic and remarkable results are typical of the whole Reynolds number range.

2.3 Effect of Isolated Roughness Elements

The roughness elements are obtained by applying "rub-on" symbols from transfer sheets commonly used in the graphic arts. Geographics Inc. manufactures a large variety of symbols which includes a convenient range of sizes of circular dots. The dimensions of the applied elements are carefully calibrated by repeatedly applying them to an aluminum block. The applied elements are carefully measured using a dial-indicator displacement gauge and a profilometer. The average height of the elements is 6 μm. Note that earlier reports indicated a height of 9 μm, based on preliminary measurements. The surface of the elements is uneven, with thickness variations on the order of 20%. Taller elements are created by stacking the 6 μm dots. Careful measurements indicate a mean thickness of 6 μm per layer, with very little compression of the lower layers. The sides of the elements are not perfectly straight because the pressure applied during installation spreads the material slightly at the edges.

When a 6 μmm roughness element (3.7 mm diameter) was re-introduced at x/c = 0.023, local transition returned to its original upstream location at x_{tr}/c = 0.40. Preliminary reports on this work contained a misprint which identified the roughness location as x/c = 0.04. The value x/c = 0.023 reported here is the correct position.

Moreover, naphthalene flow visualization reveals that the early transition occurs in the vicinity of the particular stationary crossflow vortex which passes near the roughness location. Roughness elements were placed along the chord direction and it was found that transition was not influenced. Thus, the roughness effect seems to be confined to a small region near the attachment line where crossflow disturbances first begin to be amplified. This justifies *a posteriori* the use of naphthalene in the mid-chord region.

Sound, along with 2-D and 3-D roughness (following Saric et al. 1991 for 2-D boundary layers), has no observable effects on transition. This further substantiates the role of the stationary crossflow wave.

In order to fully characterize the effect of isolated roughness near the attachment line, a variety of roughness sizes are introduced at x/c = 0.023. Roughness diameters, D, ranged from 0.3 mm to 3.7 mm, which corresponds to 0.08 to 0.5 times the stationary crossflow vortex spacing. Heights varied between 6 μm and 36 μm. The roughness Reynolds number, Re_k, based on roughness height and local velocity ranged from 0.12 to 4.5. Flow visualization measurements reveal a strong dependence of transition location on both the roughness height and the roughness diameter as shown in Figure 2. The transition location moves forward for the larger diameters and heights, and moves downstream as the roughness size is reduced. However, Figure 2 also shows that once the roughness diameter becomes smaller than about 0.1 times the vortex spacing, the transition returns to the x/c = 0.7 (pressure minimum) location, and is not influenced by the roughness, even as the height is increased. This may be because at these small diameters, the roughness induces no net streamwise vorticity on the scale of the stationary vortices.

2.3.1. Roughness Diameter

The effect of roughness diameter on the transition location is repeated at three different unit Reynolds numbers. The results are shown in Figure 3. This figure shows transition Reynolds number versus roughness diameter. It is apparent that for small roughness diameters, the transition Re returns to the clean-surface value. It is clear that the dependence of transition on Re_c is not really a unit-Reynolds-number effect, but instead is an Re_k effect.

These measurements illustrate the importance of spanwise scale, vis à vis with λ_{CF}, in assessing the role of surface roughness. Note that these conclusions are for $Re_k < 4.5$. Obviously, small diameter but larger roughness heights (like paint specks) could cause early transition.

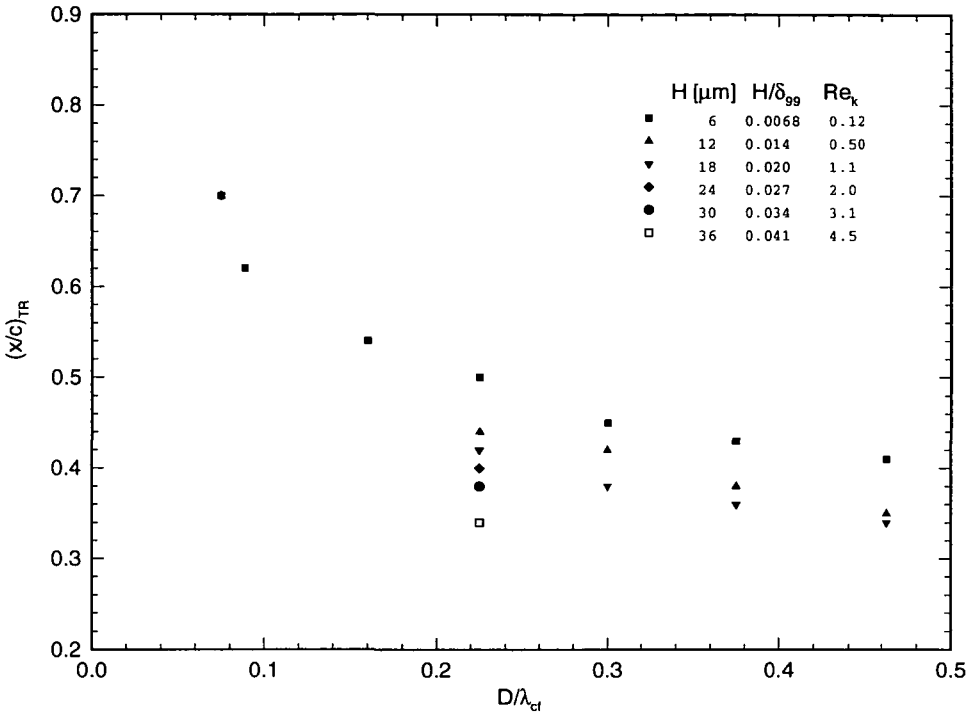

Figure 2. Naphthalene visualization results showing location of transition wedge behind the applied roughness elements. Roughness is at $x/c = 0.023$. Re_c = 2.6 x 10^6. α = -4°.

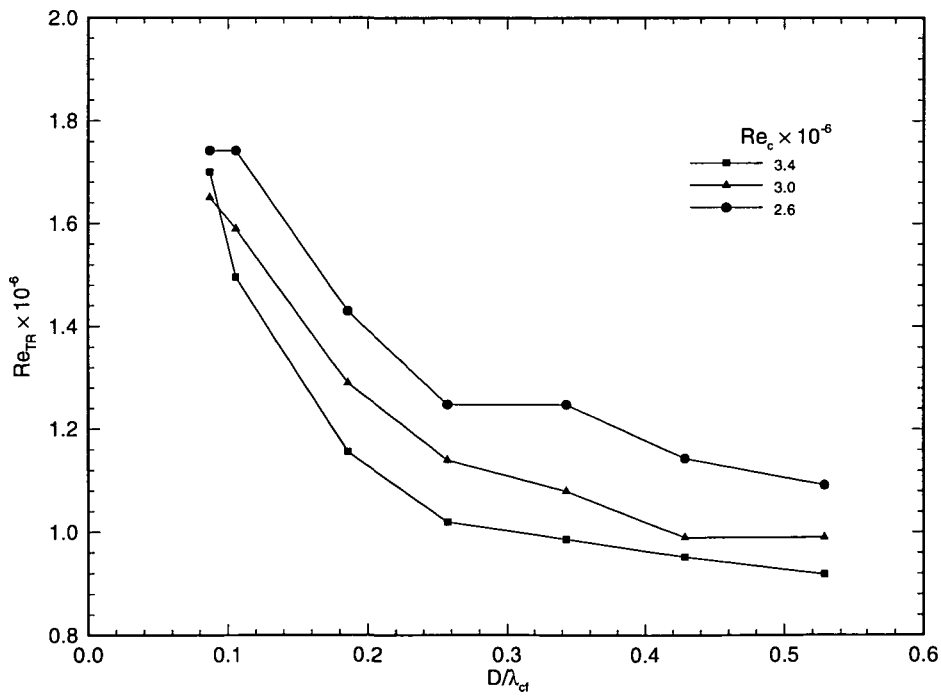

Figure 3. Variation of transition Reynolds number with roughness diameter. Roughness is at x/c = 0.023. Roughness height is 6 μm. α = -4°.

2.3.2. 3-D Roughness Location

The effect of roughness location is determined by systematically applying single 6 mm elements at chord locations between x/c = 0.005 and x/c = 0.045. Figure 4 clearly shows that the transition location is very sensitive to the roughness position. For the data shown, the attachment line is at x/c = 0.007 and the neutral point is at x/c = 0.02. When the roughness is located upstream of the neutral point, the crossflow modes influenced by the roughness will initially decay, so the influence of the roughness is minimized. For roughness too far downstream of the neutral point, the influence is also minimized, with roughness beyond x/c = 0.04 having no effect on the transition location at least for Re_k < 4.5. This quantitatively justifies the early comments about the role of roughness in the mid-chord region.

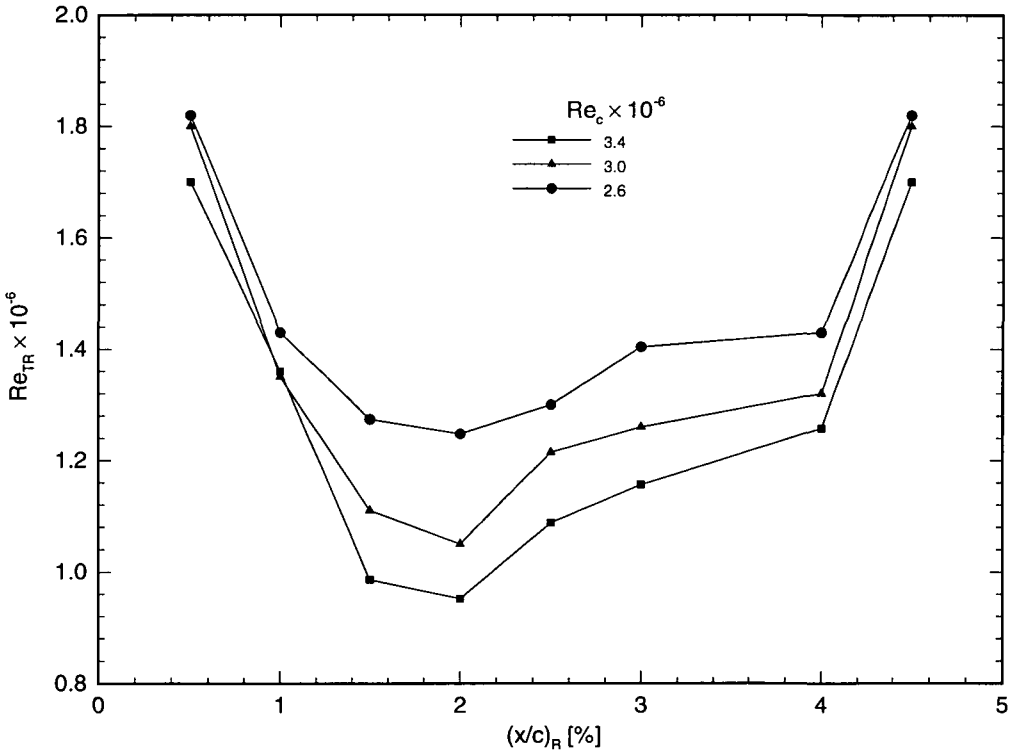

Figure 4. Variation of transition Reynolds number with roughness position.

2.4 Comparison with 2-D Boundary Layers

In the case of 2-D boundary layers (either unswept wings or swept wings in the mid-chord and weak dp/dx) small 3-D roughness does not directly influence the T-S instability. Here, 2-D roughness is more important as a receptivity mechanism (Saric et al. 1991).

The von Doenhoff and Braslow (1961) collection of data, refers only to cases where the 3-D roughness directly trips a transition wedge. As such, it is basic-state independent

since transition is occurring due to a *wake instability* of the flow behind the roughness element (they refer to this as T-S but it is neither T-S nor crossflow). Hence, because much of the data are taken from 2-D boundary layers, only the "direct trip" mechanism is recorded and any influence on the linear stability part of the process is *by-passed.* In contrast, the present results show how roughness influences the linear stability part of crossflow-vortex amplification.

2.5 Summary

We have shown that micron-sized roughness can strongly influence crossflow-dominated transition and the effect of roughness height and roughness diameter is quantified. This effect is confined to roughness near the attachment line and is not influenced by sound. Moreover, there exists a critical size below which the roughness has no effect. Detailed hot-wire measurements confirm the excitation of neighboring vortices as predicted by Mack (1985).

3. DESIGN CONSIDERATIONS

3.1 Design of the Model

After completion of the roughness experiments, a student, Mr. Mark Reibert, was trained to carry out the design of a HLFC experiment for the NASA-Ames 11-foot tunnel. The procedure followed that of the benchmark work of Saric et al. (1990) and Dagenhart et al. (1989, 1990) in that a systematic stability analysis accompanied the airfoil design consistent with the tunnel operating conditions. The airfoil design, which resulted in the new airfoil, was based on the already successful experiments at ASU. We designed the transition model that can incorporate suction to have the capabilities for (1) pure crossflow in accelerated flow, (2) combined weak crossflow and weak T-S in a flat C_p, (3) strong T-S and weak crossflow in the pressure recovery region, and (4) very strong T-S and strong crossflow in the pressure recovery region. In order to minimize difficulties with the adaptive-wall liners over most of the parameter space, the zero-lift condition (α = -3°) was designed for strongly-amplified C-F waves.

Figure 5 shows the airfoil profile and the C_p for the α = -3° condition. The profile is a modification of the NACA-67, 1-015 and, as one can see from the C_p, it should generate plenty of crossflow for the experiments. Camber was added to control lift and curvature was added near the trailing edge. The chord remains at 1.83 m and the flap has been discarded. The designation for this airfoil is *ASU (67)-0315*.

The model can be made of a solid foam with a fiber-glass skin. Previous experiments (Radeztsky et al. 1993a) indicate that surface roughness need only be controlled within 10% of the attachment line so we recommend a solid aluminum insert in the suction panel region whose tolerances are carefully controlled and whose surface is polished to 0.2 μm rms. Contoured end liners are used to simulate infinite swept-wing flow conditions. The model is mounted vertically from the test-section ceiling to floor with the leading edge swept back at 45°. The liner shapes are computed using a quasi-three-dimensional modified version of the MCARF two-dimensional airfoil code which accounts for boundary-layer displacement effects and the presence of the wind-tunnel side walls. Two rows of streamwise pressure orifices, one on each side of the test region, are used to assess both chordwise and spanwise pressure gradients.

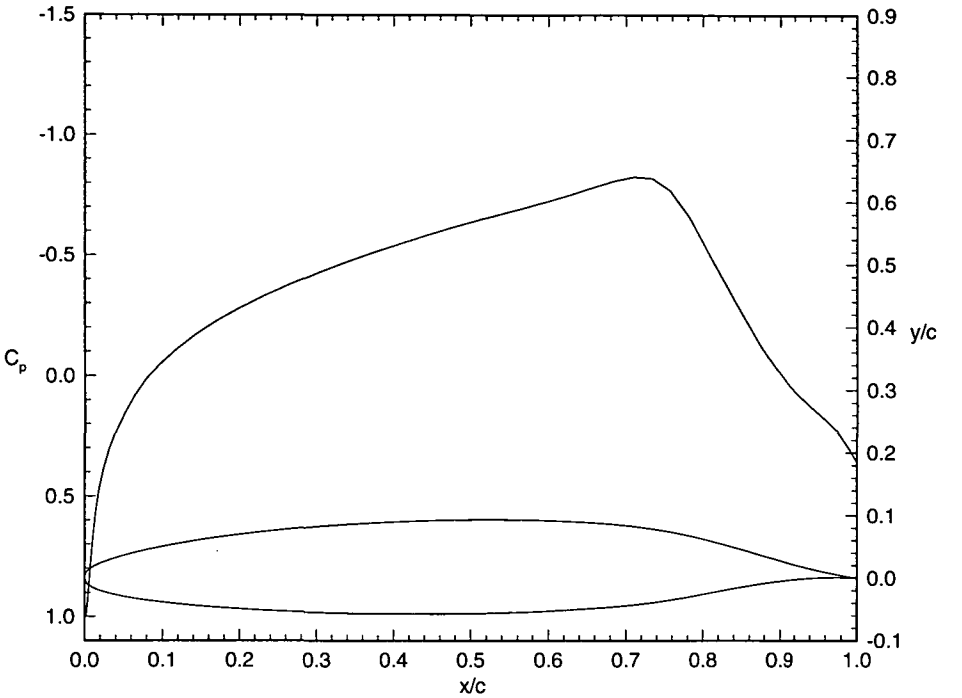

Figure 5. Profile and C_p for the ASU Suction Model: *ASU (67)-0315.* Unswept (2-D) crossection at $\alpha = -3°$

The airfoil C_p is established to control the T-S growth in the mid-chord region. The airfoil design and tunnel operating conditions will be established to assess the role of freestream turbulence in the 11-foot tunnel by overlapping with existing data in low-turbulence facilities. The roughness experiment described in some detail in Section 2 of this report is a good example of a comparative experiment.

The data of Radeztsky et al. (1993) show an insensitivity to sound in all of the important frequency ranges and hence, there are strong reasons to believe that the leading-edge roughness effects on transition will be similarly unaffected by freestream turbulence. Thus, this is the first study that should be attempted in the 11-foot tunnel. Whereas the Radeztsky et al. (1993) experiments were crossflow dominated, mixed cases of crossflow and T-S will be more important. The chord-Reynolds-number range of the 11-foot tunnel is realistic and should provide an adequate data base.

3.2 Surface Roughness Experiments

It is recommended that the same experimental procedures, established the ASU swept-wing experiment and described in Section 2, be followed for code validation and instrumentation development. The guidelines for stability experiments, outlined in Saric (1990), will also be followed.

Micro-thin hot-film gauges have been established at ASU (Mangalam et al. 1990; Glauser et al. 1994) to be suitable for transition studies. It is recommended that this instrumentation be used in the Ames experiment. At the same time, it is recommended that the NASA-Ames capability for infra-red transition detection be used.

It is recommended that the flow-field codes and the boundary-layer stability codes established at ASU be used during the experiment.

It is also recommended that the ASU Swept-Wing Model, NLF(2)-0415 be used in high-Reynolds-number tests at NASA-Ames.

Based on the success of the first phase of this program described in Sections 2 and 3.1, joint NASA-Ames/ASU experiments should be conducted on isolated and distributed roughness effects on swept-wing transition to turbulence following the work of Radeztsky et al. (1993).

4. REFERENCES

Arnal D. 1992. Laminar-Turbulent Transition: Prediction, Application to Drag Reduction. *AGARD Report 786* (Special course on skin friction drag reduction) VKI, Brussels.

Arnal, D. and Michel R. 1990. (editors) *Laminar-Turbulent Transition, Vol. III,* Springer-Verlag.

Benmalek, A. and Saric, W.S. 1994. Effects of Curvature Variations on the Nonlinear Evolution of Görtler Vortices," , *Phys. Fluids*, vol. 6 (10).

Bippes, H. 1991. Experiments on Transition in Three-Dimensional Accelerated Boundary Layer Flows. *Proc. R.A.S. Boundary Layer Transition and Control*, Cambridge, UK, ISBN 0 903409 86 0.

Bippes, H. and Müller, B. 1990. Disturbance Growth in an Unstable Three-Dimensional Boundary Layer. *Numerical and Physical Aspects of Aerodynamic Flows, Vol. IV,* Ed. T. Cebeci, Springer-Verlag, 1990.

Cousteix, J. 1992. (editor) *AGARD Report 786* (Special Course on Skin Friction Drag Reduction), VKI, March 1992.

Dagenhart, J.R. 1981. Amplified Crossflow Disturbances in the Laminar Boundary Layer on Swept Wings with Suction. *NASA TP-1902.*

Dagenhart, J.R. 1992. Crossflow Disturbance Measurements on a 45 Degree Swept Wing. *PhD Thesis,* Virginia Polytechnic Institute and State University, October, 1992.

Dagenhart, J.R., Saric, W.S., Mousseux, M.C., and Stack, J.P. 1989. Crossflow-Vortex Instability and Transition on a 45-Degree Swept Wing. *AIAA Paper No. 89-1892.*

Dagenhart, J.R., Saric, W.S., and Mousseux, M.C. 1990. Experiments on Swept-Wing Boundary Layers. *Laminar-Turbulent Transition, Vol III,* Eds. D. Arnal and R. Michel, Springer-Verlag.

von Doenhoff, A.E. and Braslow, A.L. 1961. The effect of distributed surface roughness on laminar flow. *Boundary Layer Control, Vol. II.* Ed. Lachmann, Pergamon.

Gaster, M. 1991. (editor) *Proc. Royal Aeronautical Society Conference on Boundary Layer Transition and Control*, April, 1991.

Glauser, M., Chapman, K., Dagenhart, J. and Saric, W.S. 1994. Application of Multipoint Correlation Techniques to Aerodynamic Flows. *AIAA Paper No. 94-2278.*

Hussaini, Y. and Voigt, R.G. 1990. (editors) *Proc. ICASE/NASA Langley Research Center Workshop on Instability and Transition*, Springer Verlag.

Kohama, Y., Saric, W.S., and Hoos, J.A. 1991. A High-Frequency Secondary Instability of Crossflow Vortices that leads to Transition. *Proc. R.A.S. Boundary Layer Transition and Control*, Cambridge, UK, ISBN 0 903409 86 0.

Lin, N., Reed, H.L. and Saric, W.S. 1991. Leading-edge receptivity: Navier-Stokes Computations. *Proc. R.A.S. Boundary Layer Transition and Control*, Cambridge, UK, ISBN 0 903409 86 0.

Mack, L.M. 1985. The Wave Pattern Produced by a Point Source on a Rotating Disk. *AIAA Paper No. 85-0490.*

Mangalam, S.M., Maddalon, D.V., Saric, W.S., and Agarwal, N.K. 1990. Measurements of Crossflow Vortices, Attachment-Line Flow, and Transition Using Microthin Hot Films. *AIAA Paper No. 90-1636,* June 1990.

Morkovin, M. V. 1983. Understanding transition to turbulence in shear layers - 1983. AFOSR Final Report, Contract F49620-77-C-0013.

Radeztsky, R.H. Jr., Kosorygin, V.S., and Saric, W.S. 1991. Control of T-S waves with freestream sound and 2-D roughness. *Bull. Am. Phys. Soc., vol. 36,* 2629.

Radeztsky, R.H. Jr., Reibert, M.S., Saric, W.S. and Takagi S. 1993. Effect of Micron-Sized Roughness on Transition in Swept-Wing Flows. *AIAA Paper No. 93-0076.*

Radeztsky, R.H., Jr., Reibert, M.S., and Saric, W.S. 1994. Development of Stationary Crossflow Vortices on a Swept Wing. *AIAA Paper No. 94-2373.*

Reed, H.L. and Fuciarelli, D.A. 1991. Analysis of high-frequency secondary instabilities in three-dimensional boundary layers. *Bull. Am. Phys. Soc., vol 36,* 2630.

Reed, H.L. and Saric, W.S. 1989. Stability of Three-Dimensional Boundary Layers. *Ann. Rev. Fluid Mech. vol. 21,* 235.

Reed, H.L., Stuckert, G.K. and Haynes, T.S. 1992. Stability of Hypersonic Boundary-Layer Flows with Chemistry. *Proc. AGARD Symp. on Hypersonics,* Torino, Italia, May 1992.

Reshotko, E. 1984. (editor) *AGARD Report No. 709* (Special course on stability and transition of laminar flows) VKI, Brussels, March, 1984.

Saric, W.S. 1985a. Boundary-Layer Transition: T-S Waves and Crossflow Mechanisms. *Proc. AGARD Report No. 723,* (Special course on aircraft drag prediction and reduction), VKI, Belgium.

Saric, W.S. 1985b. Laminar Flow Control With Suction: Theory and Experiment. *Proc. AGARD Report No. 723,* (Special course on aircraft drag prediction and reduction), VKI, Belgium.

Saric, W.S. 1986. Visualization of different transition mechanisms. *Phys. Fluids, vol. 29,* 2770.

Saric, W.S. 1990. Low-speed experiments: requirements for stability measurements. *Instability and Transition, vol I,* (eds. M. Y. Houssaini and R. G. Voigt) Springer-Verlag, New York.

Saric, W.S. 1992. Laminar-Turbulent Transition: Fundamentals. *AGARD Report 786* (Special course on skin friction drag reduction) VKI, Brussels, Mar 1992.

Saric, W.S. 1994. Physical Description of Boundary-Layer Transition: Experimental Evidence. *Progress in Transition Modelling, AGARD Report 793,* Ed. W.S. Saric, March 1994.

Saric, W.S. 1994. Görtler Vortices. *Ann. Rev. Fluid Mech. Vol 26,* pp 379-409.

Saric, W.S. 1995. Low-Speed Boundary Layer Transition. *Transition: Experiments, Theory & Computations.* Eds. T.C. Corke, G. Erlebacher, M.Y. Hussaini, Oxford, 1995.

Saric, W.S. and Nayfeh, A.H. 1977. Nonparallel stability of boundary layers with pressure gradients and suction. *AGARD CP 224.*

Saric, W.S., Dagenhart, J.R., and Mousseux, M.C. 1989. Experiments in Swept-Wing Transition. *Numerical and Physical Aspects of Aerodynamic Flows, Vol. IV,* Ed. T. Cebeci, Springer-Verlag, 1990, 359 (first appeared Jan. 1989).

Saric, W.S., Krutckoff, T.K., and Radeztsky, R.H. 1990. Visualization of Low-Reynolds-Number Flow Fields Around Roughness Elements," *Bull. Amer. Phys. Soc., vol. 35,* 2262.

Saric, W.S., Hoos, J.A., Radeztsky, R.H., and Kohama, Y. 1991. Boundary-layer Receptivity of Sound with Roughness. *Boundary Layer Stability and Transition to Turbulence, FED-Vol. 114*, Eds: D.C. Reda, H.L. Reed, R. Kobayashi, ASME.

Somers, D. M. and Horstmann, K.H. 1985. Design of a Medium-Speed Natural-Laminar-Flow Airfoil for Commuter Aircraft Applications. *DFVLR-IB/29-85/26.*

Spencer, S.A., Saric, W.S. and Radeztsky, R.H. Jr. 1991. Boundary-layer receptivity: Freestream sound and 3-D roughness. *Bull. Am. Phys. Soc. vol. 36*, 2618.

Thomas, A. S. W. 1985. (editor) *AGARD Report No. 723* (Special course on aircraft drag prediction and reduction) VKI, Brussels, May, 1985.